Advanced Optical Technologies

TYPE Original Research
PUBLISHED 05 July 2024
DOI 10.3389/aot.2024.1422695

OPEN ACCESS

EDITED BY
Luca Varani,
Université de Montpellier, France

REVIEWED BY
Suchita Y.,
Guru Ghasidas Vishwavidyalaya, India
Sercan Aygun,
University of Louisiana at Lafayette, United States

*CORRESPONDENCE
Karol A. Stasiewicz,
karol.stasiewicz@wat.edu.pl

RECEIVED 24 April 2024
ACCEPTED 04 June 2024
PUBLISHED 05 July 2024

CITATION
Niewczas M, Stasiewicz KA, Przybysz N, Pakuła A, Paczesny J, Zbonikowski R, Dziaduszek J, Kula P and Jaroszewicz LR (2024), Technology and research on the influence of liquid crystal cladding doped with magnetic Fe_3O_4 nanoparticles on light propagation in an optical taper sensor.
Adv. Opt. Technol. 13:1422695.
doi: 10.3389/aot.2024.1422695

Technology and research on the influence of liquid crystal cladding doped with magnetic Fe_3O_4 nanoparticles on light propagation in an optical taper sensor

Michał Niewczas[1,2], Karol A. Stasiewicz[1]*, Natalia Przybysz[1], Anna Pakuła[1,2], Jan Paczesny[3], Rafał Zbonikowski[3], Jerzy Dziaduszek[1], Przemysław Kula[1] and Leszek R. Jaroszewicz[1]

[1]Faculty of Advanced Technologies and Chemistry, Military University of Technology, Warsaw, Poland, [2]Institute of Micromechanics and Photonics, Warsaw University of Technology, Warsaw, Poland, [3]Institute of Physical Chemistry, Polish Academy of Sciences, Warsaw, Poland

The results obtained for new dual-cladding optical fiber tapers surrounded by liquid crystal (LC) doped with Fe_3O_4 nanoparticles in a specially developed glass cell are presented. The created structures are sensitive to changes in refractive index values in the surrounding medium caused by modifying external environment parameters. In this investigation, cells are filled with nematic LCs 6CHBT and with the same mixture doped with 0.1 wt% and 0.5 wt% of magnetic nanoparticles (Fe_3O_4 NPs). The taper is made on a standard single-mode telecommunication fiber, stretched out to a length of 20.0 $\pm$ 0.5 mm, and the diameter of the tapers is approximately 15.0 $\pm$ 0.3 µm, with a loss lower than 0.5 dB @ 1,550 nm. Measurements are carried out in a wide range covering the visible and infrared ranges in two setups: 1) without a magnetic field, with steering only by voltage and 2) with an applied magnetic field. The presented spectrum results are divided into two ranges according to the parameters of optical spectrum analyzers: 350–1,200 nm and 1,200–2,400 nm. For all investigations, a steering voltage is chosen from the range of 0 to 200 V, which allows for establishing the influence of dopants on transmitted power and time response at different arrangements. Due to the sensitivity of LCs to temperature changes, this paper focuses on measuring at room temperature the effect of the magnetic field on propagation in a fiber optic taper. The proposed solution demonstrates the technology for creating advanced components as a combination of fiber optic technology, LCs, and nanoparticles. The presented results show the possibility of creating new sensors of various external factors such as magnetic or electric fields in miniaturized dimensions.

KEYWORDS

tapered optical fiber, liquid crystals, optical fiber device, magnetic nanoparticles, fiber technology

10.3389/aot.2024.1422695

1 Introduction

Fiber optic technology is being rapidly developed for high-speed data transfer, especially sensing applications. We are looking for a "new material" to improve the device parameters or increase its sensitivity. Fiber optics as sensors or sensor elements are used in almost all areas of life, which include medicine (Baldini et al., 2008; Ahamed et al., 2010; Zhang et al., 2022), energy conversion (Lohse and Murphy, 2012; Huang et al., 2020), environmental monitoring (Al-Qazwini et al., 2015; Butt et al., 2022; Kurzych et al., 2022), civil engineering (Guo et al., 2021; Kurzych et al., 2020), industrial production (Li-hui and Junfeng, 2023), aerospace (Taha et al., 2021), food safety (Chen et al., 2020), and telecommunication (Dudek et al., 2014). This development and the requirement to find new sensing solutions also require the search for new materials that will improve or change the properties of current sensors. As a result, modified materials are produced with new properties called hybrids (Nealon et al., 2012; Hsu et al., 2017; Škarabot et al., 2018). The use of extra materials surrounding the fiber creates possibilities for applications due to light–matter interaction, that is, the change of material properties manifests in the shifting of propagated light characteristics like amplitude (Kim et al., 2019) or spectral shifts (Li, 2020). One of the exciting solutions that scientists are paying a lot of attention to is combining fiber optic technology with LCs technology (Woliński et al., 2017; Markos et al., 2017) and nanomaterials (Blanc et al., 2022; Korposh et al., 2019).

The standard optical fiber technology has excellent resistance to external interference in a measurement environment, which makes it reliable and stable, and enables it to be used in many applications in different places. However, to achieve a higher sensitivity and broadband detection function, special processing procedures are applied to modify the geometry of the fiber to allow light interaction with an external material, which amplifies the detecting signals. The processing methods include taper pulling, core-offset splicing, laser etching, and side grinding and polishing (Zhao et al., 2019; Fu et al., 2022). The first one is the most popular technique based on flame heating and simultaneously stretching and decreasing the diameter of the fiber. The taper optical fiber (TOF) technology does not require complex processing and expensive materials, and the preparation cost is relatively low (Stasiewicz et al., 2022a). The process of manufacturing is easy to control with high repeatability. Owing to their structure, it is possible to manufacture different transducers by changing their angular structure, sensing medium, and sensing layer. It should be mentioned that a standard optical fiber propagation of light is associated with an appropriate selection of materials forming the cladding and core, with an appropriate refractive index n_{core}, $n_{cladding}$ filling the Maxwell equation/condition. The light beam can be propagated in two ways: based on the phenomena of total internal reflection (TIR) in classic fibers or the principle of photonic bandgap in photonic crystal fibers (PCFs) (Katsunari, 2006). The change in the refractive index of materials causes the modification of properties of the propagated light in the form of modes. The value of normalized frequency V determines the number of modes propagating in the fiber and the losses. This parameter, Eq. 1, is described as (Brambilla, 2010)

$$V^2 = a\frac{2\pi}{\lambda}\sqrt{{n_{core}}^2 - {n_{cladding}}^2}. \quad (1)$$

From the above formula, it can be concluded that the wavelength (λ) and the core diameter (a) also influence the number of modes propagating in the fiber. These parameters are connected with the phenomenon of evanescence wave. Owing to the TOF, the diameter of the core and cladding can be controlled to expose the evanescing field to the outer sensitive coating surrounding the TOF area. It is directly related to the change in the standard optical fiber geometrical parameters during the tapering technological process (Brambilla, 2010). As the optical fiber is pulled out, the diameter of the fiber is reduced, and thus, the part of the evanescent field emerging in different regions of the TOF changes simultaneously. The most sensitive area and the most important from the sensing point of view in a taper is the waist region, that is, where the evanescent field is the largest; see Figure 1.

As the diameter of the optical fiber decreases, an increase in the diameter of the modulus field is noticeable. In the fiber's waist area, the structure is completely filled, and interacts with the external environment, as shown in Figure 1. By adding a new material, we can change parameters such as absorption or the refractive indices (RIs) and affect the propagation of the beam inside the fiber (Stasiewicz et al., 2022a; Brambilla, 2010).

The evanescent field is related to the penetration depth parameter (d_p) (i.e., how deeply the light beam penetrates the cladding), which depends on the wavelength (λ) and the value of the core and cladding refractive index (RI – n_{core}, $n_{cladding}$) for a standard fiber before the tapering process; the penetration depth is described by the formula presented in Eq. 2, (Brambilla, 2010; Tian et al., 2011):

$$d_p = \frac{\lambda}{2\pi\sqrt{{n_{core}}^2\theta_i - {n_{cladding}}^2}}, \quad (2)$$

where θ_i corresponds to the angle of incidence of a plane wave on the core/cladding interface.

In the taper waist area, the RI of the TOF and the RI of the sensitive coating should be considered to estimate the d_p value. This evanescence field effect observed in the TOF allows the use of an extra material in the taper surroundings, forming a double-clad structure (Wang et al., 2018; Tiwari et al., 2017). Due to the described phenomenon, it is possible to influence the light parameters by changing the boundary conditions by replacing/creating new cladding with different chosen materials.

The exploration of new opportunities to control light beam propagation or influence its parameters requires using new materials or creating mixtures of well-known materials. The investigation focused on ways to control light's optical parameters using LCs as found in Moś et al. (2022) and Lacková et al. (2024). As it is well known, LCs (Jadżyn et al., 2010; Sengupta, 2013) are built of elongated molecules, allowing to determine their anisotropic properties such as ordinary n_o and extraordinary n_e RIs. Depending on the alignment of the molecules to the light beam propagation direction, a different RI value is detectable. LC molecules can be easily reoriented by using an appropriate electrical field (higher than the threshold voltage), temperature (changes in structure), and magnetic field.

When looking for new possibilities for light beam control, the authors have considered the possibilities of controlling optical beam parameters using a magnetic field to especially change and control the light beam parameters in the optical fibers' element.

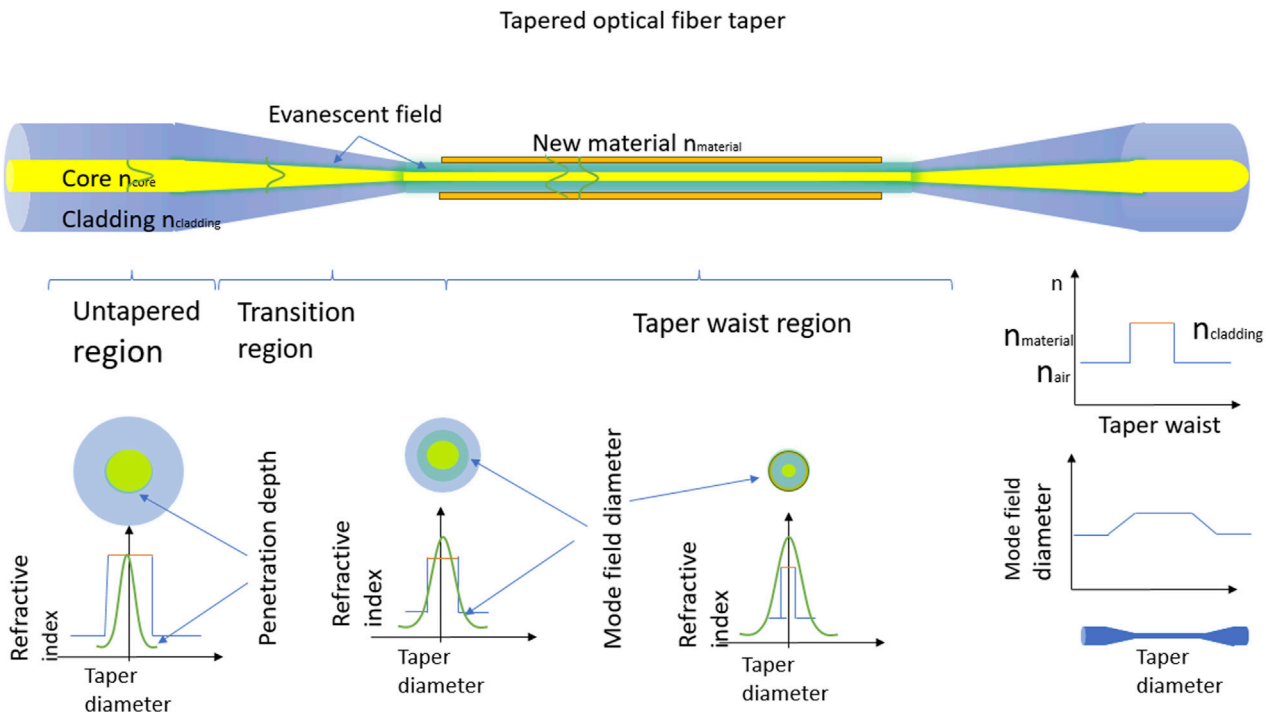

FIGURE 1
Scheme of the TOF with selected main parameters and the visualization of change of evanescence filed along the taper.

Many works have reported on fully filling air holes of a PCF with magnetic fluid (Miao et al., 2011; Dufour et al., 2020), polymers (Frazão et al., 2008) or pure LCs (Larsen et al., 2003; Larsen et al., 2003), or on surrounding tapers with magnetic fluid (Luo et al., 2015; Shi et al., 2017; Layeghi and Latifi, 2018; Shi et al., 2018; Stasiewicz et al., 2022b), as a detector of different acids (Das et al., 2022), magnetometers (Chen et al., 2019), or magnetic field sensors (Zheng et al., 2015). Most of these use changes in the effective RI of the cladding structure (in tapers or air holes) and hence effect a change in the propagation properties (Larsen et al., 2003). In this article, we would like to show the possibilities and effects of light beam steering by using nematic LCs doped by different nanoparticles (Moś et al., 2022; Lacková et al., 2024). Referring to previous work with nanoparticles (Moś et al., 2022; Stasiewicz et al., 2022b), the authors have decided to focus on Fe_3O_4 nanoparticles (Petcharoen and Sirivat, 2012). The combination of these three elements/materials has many benefits: the use of optical fibers over long distances, miniaturization of the device, tunability of the device to a different wave range, and low manufacturing costs, as well as the possibility to react with a magnetic field.

The use of TOF and LCs has been known for many years (Veilleux et al., 1990; Petcharoen and Sirivat, 2012; Korec et al., 2019). It was possible to control LCs, but only at high threshold voltages, and the LC cells were characterized by very high thicknesses. Nowadays, the newly developed technology associated with improving parameters is used as a novelty—the use of appropriate spacers close to the diameter of the taper waist, use of the optimal type of LC, or use of a mixture of LC with other materials such as NPs. Research was carried out on the influence of doping with Fe_3O_4 NPs to LC and on how the propagation parameters change upon application of the magnetic field. Our research team has investigated how NPs with LC affect light propagation in the optical fiber and what occurs after being put in a cell in a magnetic field. The results show how to elaborate a new kind of device working in a different wavelength range and be modified by different factors— electric or magnetic fields, or both. In the research, LCs named 6CHBT were tested. The tests were conducted on cells with pure LCs and a mixture of Fe_3O_4 NPs dispersed in the LCs. Thus, we can compare the results of adding NPs to light propagation under voltage and temperature control. Tapers were manufactured from standard telecommunication single-mode fibers (SMFs) with a cutoff wavelength of 1,260 nm (diameter of cladding: 125 μm, core of approximately 9 μm)—the most popular and low-cost material produced by Corning®.

The next part of the article describes different kinds of materials that were used for manufacturing the cell like 6CHBT nematic LCs, Fe_3O_4 nanoparticles, the procedure of mixing them, and the technology of manufacturing the double-clad adiabatic taper as the base element of the created devices and build measurement systems for the investigation of sensors.

2 Materials and methods

2.1 Propagation of light in TOF with and without LC cladding

The description of beam propagation in optical fibers is well known and has been widely described in the literature (Katsunari,

2006). The main feature of such a propagation is the guidance of light inside a cylindrical core structure with an RI higher than that of the surrounding sheath. The choice of RI differences determines the losses and modality inside the fiber. For the wave description, Maxwell's equations are standardly used (Katsunari, 2006). As the introduction states, a part of the power is propagated at the boundary of the two media as a fading wave, which, in the absence of a sheath, would be sensitive to changes in the external environment conditions.

This article's introduction describes many ways to remove/modify the sheath, giving direct access to the wave propagating in the optical fiber's core. Here, bilateral constriction technology was used to heat the fiber in a low-pressure gas torch using a propane–butane oxygen mixture. The result of the tapering of fibers was a change in core and cladding diameters, as well as an increase in the mode field, which, for the taper waist, filled the entire structure while interacting with the materials surrounding the taper (Figure 1).

The change in boundary conditions is also directly related to the change in optical fiber dimensions. The light is not propagated at the core/cladding interface but at the air/new cladding interface. The approximations used in the mode solutions for a standard optical fiber, where the difference in RIs is very small, are not applicable. The light beam interacts with the structure's surroundings in the TOF. The light beam propagates in a whole taper structure, which becomes the new core of the structure, and the surroundings become a cladding. Due to the difference between the mediums and the diameter of the taper waist, it should be mentioned that the created structure possesses multimode propagation (Brambilla, 2010). The transition regions are responsible for light transformation from and to non-tapered regions. As described above, the phenomena in an optical fiber taper structure are used to create new devices that influence light propagating inside by changing the external materials with variable properties depending on different factors, e.g., oil detection (Li-hui and Junfeng, 2023), biosensors (Tian et al., 2011), and temperature (Wang et al., 2018). The connection of the TOF with various materials has been widely described and used to build sensors, filters, and amplifiers (Tian et al., 2011; Tiwari et al., 2017; Wang et al., 2018; Moś et al., 2022).

Our previous paper focused on a detailed analysis of the changes in the propagation of the light beam in a fiber optic conductor provided by LC mixtures acting as a fiber optic cladding. The anisotropic properties of LCs (Jadżyn et al., 2010) cause the possibility of changes in the RI depending on the orientation of the molecules, which can be altered by external parameters such as temperature and electric or magnetic fields. It should also be mentioned that LCs have a higher RI than do fiber optics, which determines that light uses the bandgap propagation mode (Larsen et al., 2003; Larsen et al., 2003). In addition, the substrates with orientation layers that make up the cell act as additive resonant surfaces, which causes some of the light to reflect off them and can be coupled back to the fiber cone. In a standard SMF, the basic mode is propagated. When we tapered such a fiber, the boundary conditions changed, and in propagation, we observed many modes, especially in the taper waist area. The fundamental mode began to be coupled with cladding modes, so the light beam was modified. The light leaked from the taper's structure to the LC cladding.

Here, an additional modification was made by doping the LC with magnetic Fe_3O_4 NPs (Miao et al., 2011; Larsen et al., 2003). This allowed for enhancing the possibility of controlling the magnetic field of selected parameters inside the LC structure, particularly the orientation of molecules and their rotation.

2.2 LCs and NP materials

The starting material is a nanocomposite based on an LC mixture with metal NPs, allowing for the study of optical and electro-optical properties. Liquid crystalline material with a positive $\Delta\varepsilon$ permeability value was used. The material is the nematic LC 6CHBT (1-(4-hexyl-cyclohexyl)-4-isothiocyanato-benzene) of the formula $C_{19}H_{27}N_1S_1$ with the transition temperature from the nematic phase to the isotope phase at 42.8°C. In addition, this compound has a positive optical birefringence value of Δn = 0.16. Table 1 presents the basic parameters of 6CHBT (Jadżyn et al., 2010; Sengupta, 2013). The parameter worth paying attention to is the LC RI, which, in terms of value, is higher than the RI of silica (at room temperature).

The above-described LC material was doped with ferromagnetic NPs, with 0.1% and 0.5% weight concentrations of Fe_3O_4 NPs in LC. For the prepared samples, we did not observe agglomeration of NPs in the volume of the mixture or optical losses during the research. Measurements were carried out at room temperature and were focused on the influence of the magnetic field, without testing for a change of LC properties in a different temperature of LC such as the isotropic state. Previous articles and measurements have described the influence of temperature and the change of propagation from room temperature to the isotropic state (Korec et al., 2019). From the literature investigation in an isotropic state, the mixture of LC with nanoparticles causes a higher loss depending on the distribution of the nanoparticles.

The synthesis of Fe_3O_4 NPs capped with oleic acid was carried out according to the protocol published by Petcharoen and Sirivat (2012). In brief, 1.5 g of $FeCl_2 \cdot 4H_2O$ (≥99%, Sigma-Aldrich) and 5 g $FeCl_3 \cdot 6H_2O$ (≥99%, Sigma-Aldrich, CAS: 10025-77-1) were dissolved in 100 mL of deionized, ultrapure water (Direct-Q®). The mixture was heated up to 90°C with vigorous stirring and argon flow, then 0.8 mL of oleic acid (90%, Sigma-Aldrich, CAS: 112-80-1) and 10 mL of 25% $NH_4 \cdot OH$ (aqueous solution, Sigma-Aldrich, CAS: 7803-49-8) were added subsequently. The immediate color change from orange to blackish was observed. The reaction was continued (stirring, argon flow, temperature) for 15 min. After it cooled down, the magnetic precipitate was rinsed several times with deionized water and ethanol alternately. The final product was dried at 60°C or room temperature.

Such prepared Fe_3O_4 NPs were further examined. The structure of magnetite was confirmed by using Powder X-ray Diffraction (PXRD) (Petcharoen and Sirivat, 2012) (Figure 2A). The crystalline size calculated using the Scherrer equation (Scherrer, 1918) was 7.49 ± 0.07 nm. A similar diameter (approximately 10 nm) of nanoparticles was observed thanks to the scanning transmission

TABLE 1 Properties of the used LCs: 6CHBT (Jadżyn et al., 2010; Sengupta, 2013).

LC	Structure	n_e (589 nm)	n_o (589 nm)	Δn (589 nm)	$\varepsilon_\perp$ (1kHz)	$\varepsilon_{\parallel}$ (1kHz)	T_{ISO} [°C]
6CHBT	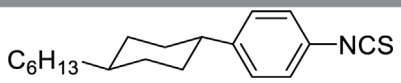	1.672	1.518	0.154	4.3	12.0	43.0

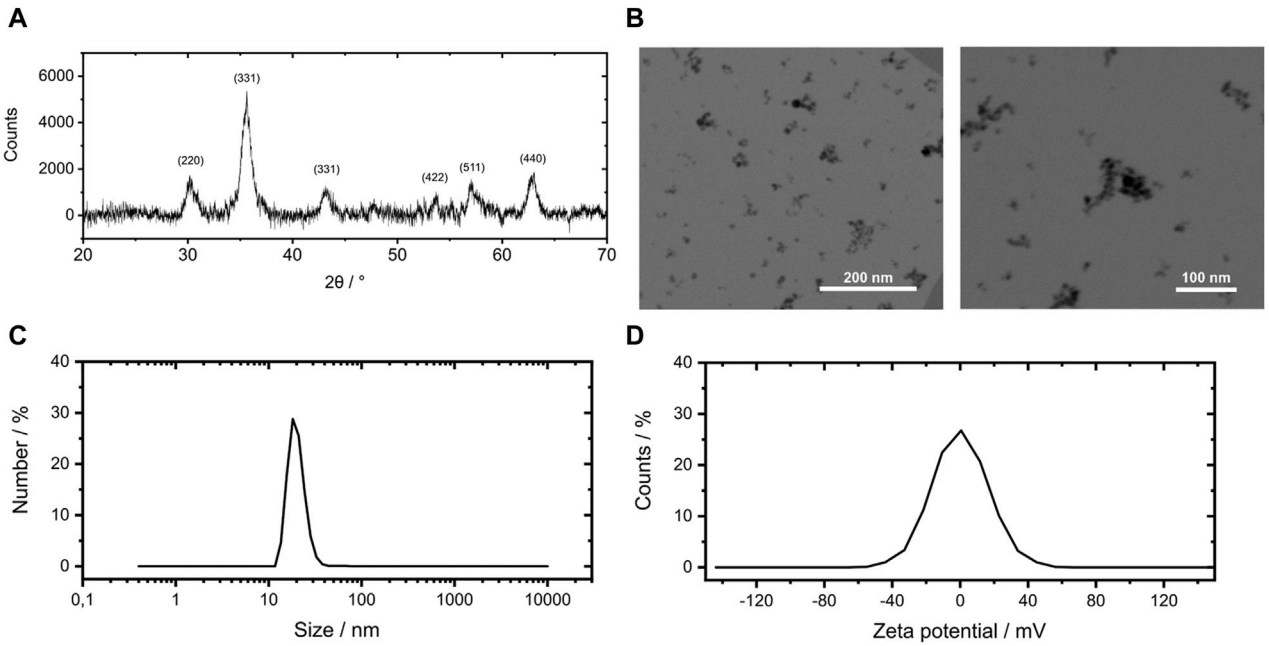

FIGURE 2
Diffractogram of synthesized Fe_3O_4 NPs capped with oleic acid. The background has been subtracted. Cu K(α) **(A)**, STEM pictures of Fe_3O_4 NPs 30 eV **(B)**, size distribution of Fe_3O_4 NPs by number, according to dynamic light scattering measurements in toluene **(C)**, and zeta potential of Fe_3O_4 NPs in toluene **(D)**.

electron microscopy (STEM) (Figure 2B). These results vary from dynamic light scattering measurements of hydrodynamic diameter in toluene (Figure 2C); however, it can be explained by partial agglomeration of the particles, visible also in STEM pictures. The average zeta potential of the nanoparticles in toluene was approximately 0 mV (Figure 2D). The prepared ferrofluid colloid in the organic phase (after solvent evaporation) served as the second component to obtain a LC nanocomposite with Fe_3O_4 NPs.

Each mixture of NPs with LC was prepared by measuring an appropriate amount, on the analytical balance, of NPs and LC, which was placed in a 1.5-mL glass vial and then stirred in an ultrasonic cleaner for 30 min at 45°C. Each sample was checked for symptoms of NP agglomerations by organoleptic observations and to further perform a size stability test of the volume using the dynamic light scattering measurement method. The appearance of agglomeration of nanoparticles in the provided research would make it impossible to carry out further stages of research.

The measurement was carried out at room temperature. Two N42 magnets with dimensions of 10 × 10 × 10 mm were used with the following parameters: remanence induction Br: 1.28–1.32 [T]; coercivity HcB: min. 923 [kA/m] coercivity HcJ: min. 955 [kA/m]; magnetic energy density (BH): max. 318–342 [kJ/m^3].

This is possible at the initial stage by means of organoleptic observation, and then to perform a size stability test of the volume by means of the dynamic light scattering measurement method.

2.3 Technology

This section presents the manufacturing of an LC cell with TOF and the arrangements for the influence of electric and magnetic fields. Fiber Optic Taper Element Technology (FOTET) was used to manufacture the tapered fibers (Figure 3A). The arrangement of the FOTET has been widely described in previous articles (Mość et al., 2022; Stasiewicz et al., 2022b). The setup allowed obtaining different shapes of tapers: adiabatic and nonadiabatic. The main advantages of preparing tapered fibers using the FOTET are full control of elongation parameters like elongation length, burner movement, and the distance from the fiber or step motor's velocity (controlled by an anti-gravity unit), and the diameter of the taper waist region. All these offer the possibility of constructing different devices without removing the manufactured taper. All procedures were controlled by computers that were enabled for the precise positioning of all elements. The optical power changes were

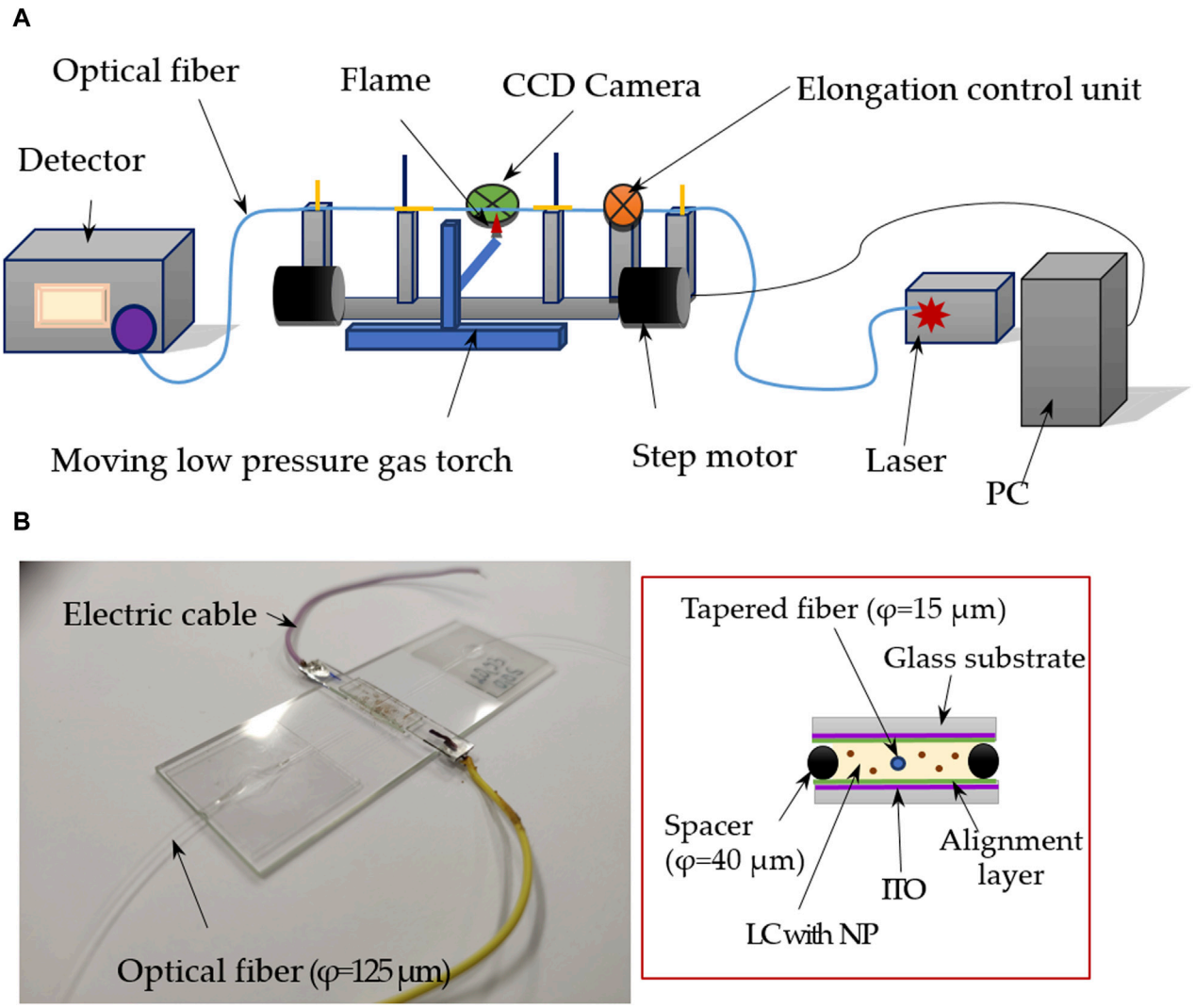

FIGURE 3
Scheme of the FOTET system arrangement for the manufactured tapered fiber **(A)** and scheme of the investigated device **(B)**.

constantly monitored during elongation using laser and a photodetector connected to the opposite ends of the fiber. Thus, attenuation after the completed tapering process could be easily calculated. The FOTET enabled the creation of devices with accuracy to single micrometers using the included charge-coupled device camera the short (CCD) and software.

The parameters of the prepared tapers were the same as for the pure LC systems presented before (Larsen et al., 2003). They were characterized by low losses below $\alpha = 0.2$ dB, which correspond to the adiabatic taper profile ensuring the least possible losses; elongation $L = 20.20 \pm 0.05$ mm; and the diameter of the taper waist $\varphi = 14.50 \pm 0.50$ μm (which means that the taper ratio is about eight times) for a wavelength of 1,550 nm that corresponds to the single-mode work of the used SMF. Such a taper in fact possesses a double-clad structure when standard cladding becomes the first part of cladding and the external environment becomes double clad.

The tapered fiber LC doped with NPs cells was prepared in the next stage. The initial arrangement of the molecules was achieved using the glass substrate covered with ITO (Indium Tin Oxide). The obtained tapered fiber was placed between two electrodes, maintaining an even gap between both the plates without touching each other. The spacers with a diameter of $\varphi = 40$ μm were used to maintain the repetitive and established distance between the electrodes. In this paper, the perpendicular arrangements of taper and electrodes were investigated. In this case, the alignment layer of the top and bottom electrodes was perpendicular in direction to the taper axis. The prepared cells were filled with pure LCs and LC doped with NPs. Filling of the prepared taper cell with LC was carried out using capillary forces. After inserting LCs with NPs into the cell, the quality of the liquid with NPs was checked under a polarizing microscope. Figure 3A presents the prepared and investigated LC cell with the taper and the cross section of the alignment of its taper (Figure 3B). As can be seen, the solution created is of small dimensions, approximately 5 × 20 mm (cell), with a thickness of $\varphi = 40$ μm, as mentioned and developed earlier (Moś et al., 2022; Korec et al., 2019). In the LC, Fe_3O_4 nanoparticles were dispersed uniformly so that the created optical taper is surrounded by them on all sides. In addition, such

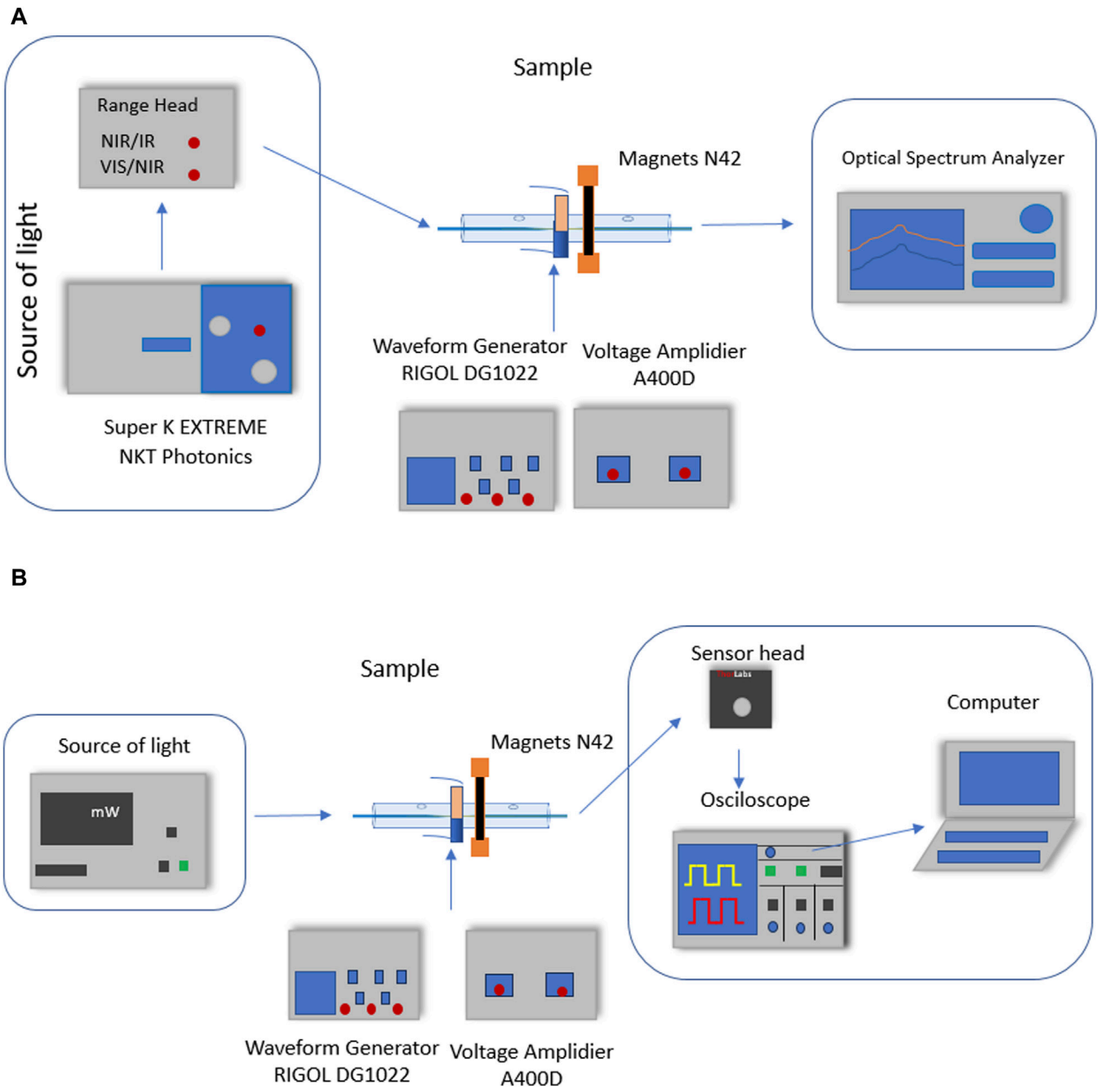

FIGURE 4
Scheme of applied arrangements for measurement: transmission in a wide range of 1,200 nm–1,800 nm **(A)** and in single-mode 1,550 nm to obtain time courses **(B)**.

dimensions of the device allow to control the magnetic field generated by standard neodymium magnets. Thanks to the small dimensions of the created device, it can be used in many solutions such as interferometric systems, fiber-optic network sensors as elements of distributed sensors, or elements modifying beam parameters.

The measurements were carried out in a few steps. The first step was connected with obtaining references of pure LCs and measuring the influence of a magnetic field on light propagation inside the taper structure. Only the medium RI, which can be described as the medium molecule director, was considered in this investigation. The second step was connected with measuring the influence of doped LC with Fe_3O_4 NPs in the range of 0.1 wt% and 0.5 wt%, chosen as the best configuration based on the literature data (Budaszewski et al., 2019; Orlandi et al., 2016). Topological defects were induced in the doped LC around NPs. Even small amounts of NPs significantly influenced bulk material properties due to intermixing NP's effects on alignment layers and bulk properties (Urbanski, 2015). For the prepared samples, we did not observe the agglomeration of NPs in the volume of the mixture and optical losses during the research. Additionally, to avoid the agglomeration of NPs, the mixture was applied right before the measures.

Samples prepared in this way were tested at two stations. The first was responsible for transmission measurements in a wide range,

10.3389/aot.2024.1422695

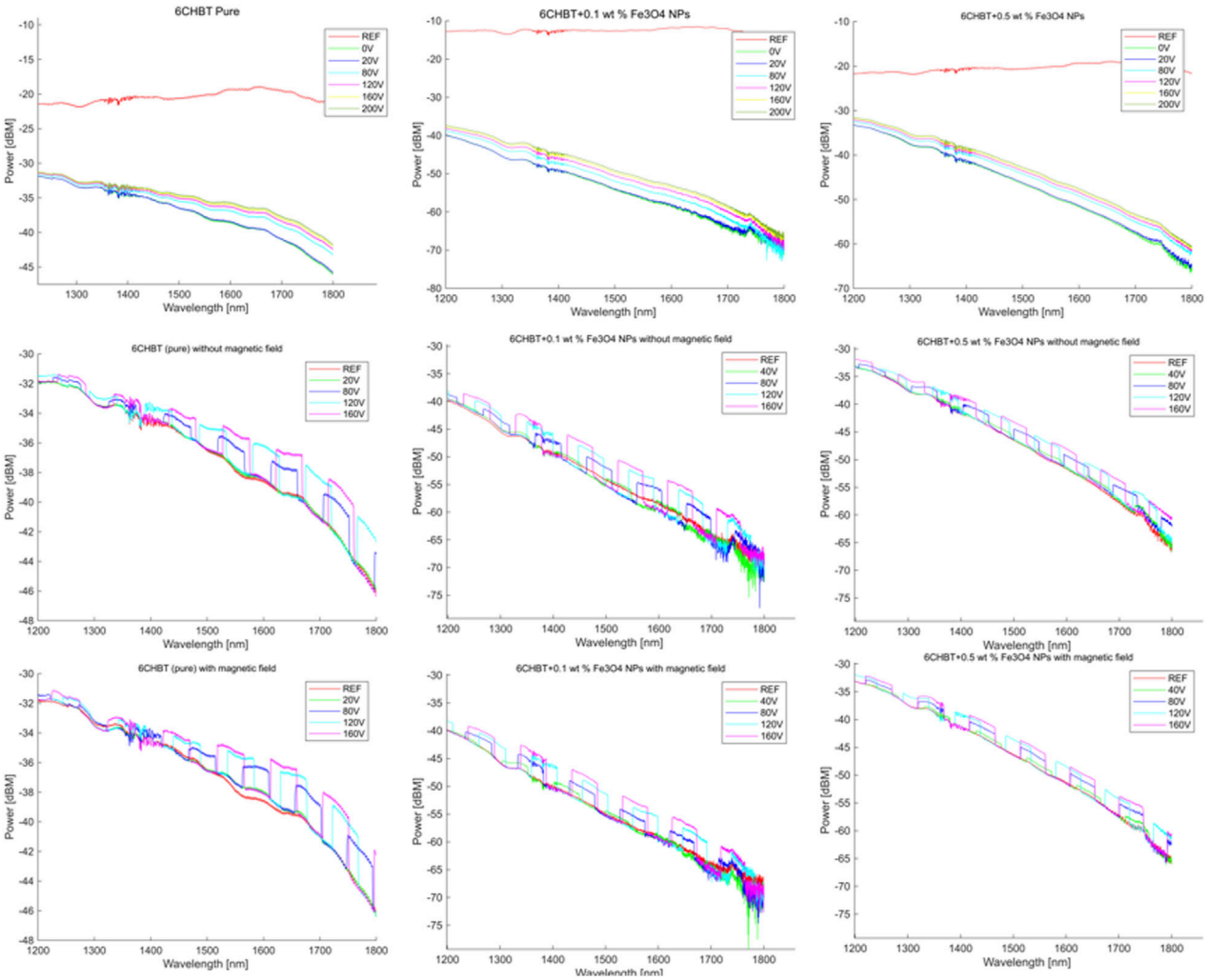

FIGURE 5
Spectra obtained for LCs: **(A)** 6CHBT (pure); **(B)** 6CHBT + 0.1 wt% Fe_3O_4 NPs; **(C)** 6CHBT + 0.5 wt% Fe_3O_4 NPs. The top row presents data under the steering voltage range U = 0–200 V without modulation and without the external magnetic field. The middle and bottom rows show spectra obtained when modulation with a frequency of 2 Hz for voltage from the range 0–180 V was applied. The middle row shows results without and the bottom with the external magnetic field applied to the system.

i.e., 1,200–1,800 nm (Figure 4A). The transmission measurement system used a broadband light source, SuperK Extreme EXR-15 (NKT Photonics, Birkerød, Denmark; operating in the 400–2,400 nm range), a splitter connected to the NKT Photonics SuperK SPLIT laser range of near-infrared (NIR)/infrared and visual/NIR, optical spectral analyzer AQ6375 (Yokogawa, Tokyo, Japan; operating in the range of 1,200–2,400 nm). Limiting the SC source range to the IR range was related to the properties of the optical fiber used, with its working length in the single-mode regime of the 1,280 nm range.

The second arrangement (Figure 4B) was built to measure the time curves for 1,550 nm. For such a wavelength, the used fiber possesses the lowest attenuation. The system consisted of the light source TSL-210V (Santec, Aichi, Japan). The InGaAs Switchable Gain Detector working in the range of 900–1,700 nm PDA10CS-EC (Thorlabs, Newton, NJ, United States) was used. The data were acquired using the digital oscilloscope DS7034 (RIGOL, Suzhou New District, Suzhou, China), waveform generator DG1022 (RIGOL, Suzhou New District, Suzhou, China), and voltage amplifier A400D (FLC Electronics, Pendulum Instruments, Malung, Sweden) for control and changes in voltage and for controlling the orientation of the LCs.

All measurements were carried out at room temperature.

3 Results

The effect of the applied voltage with an additional external magnetic field obtained by two magnets on changes in spectral characteristics and time curves was investigated. First, we evaluated the effect of pure 6CHBT LC and its influence (as cladding) on light propagating in a wide range from 1,200 nm to 1,800 nm. Figure 5 presents spectral characteristics obtained for 6CHBT (pure) (Figure 5A), 6CHBT+ 0.1 wt% Fe_3O_4 NPs (Figure 5B), and 6CHBT + 0.5 wt% Fe_3O_4 NPs with voltage steering in the range of 0–200 V without modulation

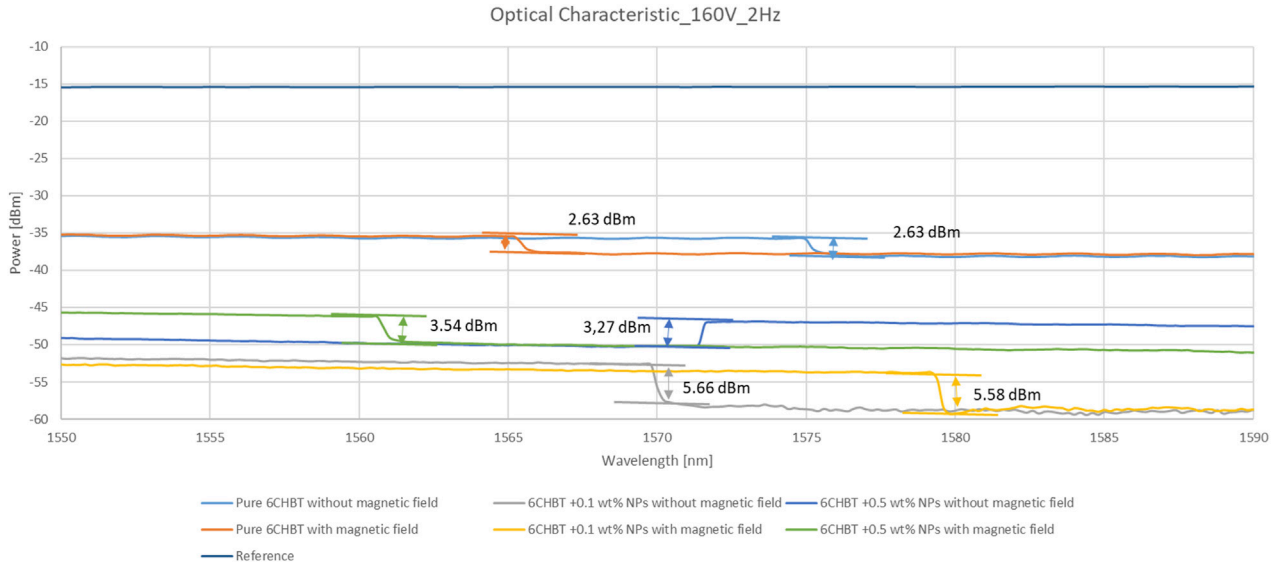

FIGURE 6
Optical characteristics were obtained for pure LCs 6CHBT, with 0.1 wt% and 0.5 wt% Fe_3O_4 NPs, without a magnetic field, and with the external magnetic field applied. The square shape of modulation with a frequency of 2 Hz for 160 V was applied.

(Figure 5C). The presented graphs show that 6CHBT LC as a new cladding causes a decrease of power in the whole range, which is connected with bandgap propagation, absorption, and dispersion of LC molecules. Power was slightly increased for pure 6CHBT, and voltage increased power in the new sensor. For a device with LC with Fe_3O_4 NPs, a slight increase of power in the whole spectral range is observed. The most visible changes were observed for LC with 0.1 wt% of Fe_3O_4 NPs. The described changes were caused by the influence of NPs, which were disparaged in a whole volume of LCs, creating new centers in which the orientation of the molecules was disturbed and, consequently, the RI associated with the alignment of the molecules had changed. For all cases, a complete reorientation of the molecules was observed over 160 V. No additional changes in RIs were observed above this value.

It should be noted that all measurements were carried out at room temperature without changing it. As is known from the literature (Woliński et al., 2017), with an increase in temperature, there is the change in RIs, and after reaching a suitable temperature, the LC from a birefringent material turns into an isotropic liquid. For this reason, at this stage of the research, the focus was on determining the influence of the magnetic field and its measurement.

The second part of the experiment focused on the connection between the spectral characteristics and the steering voltage with additional modulation of this signal with 2 Hz. During this measurement, the influence of the external magnetic field on the mixture of LC 6CHBT and magnetic NPs was investigated.

As the control voltage increased in the system without modulation, a slight increase in power was observed for the entire spectral range for pure 6CHBT, 6CHBT + 0.1 wt% Fe_3O_4 NPs, and 6CHBT + 0.5 wt% Fe_3O_4 NPs. This is associated with a complete tuning of the orientation of the molecules and a change in the RI to a lower one for which the propagation conditions allow better propagation with lower losses. The change between 0 V and 160 V reached no more than 5 dBm for approximately 1,550 nm and decreased with wavelength toward shorter wavelengths.

The middle row of Figure 5 presents spectral characteristics of pure 6CHBT, 6CHBT + 0.1 wt% Fe_3O_4 NPs, and 6CHBT +0.5 wt% Fe_3O_4 NPs for voltage steering in the range 0–160 V and modulation of 2 Hz without an external magnetic field. The bottom row of Figure 5 presents the results with the same settings with an additional external magnetic field applied.

Full reorientation of LC molecules occurs above 160 V. The next step was to measure the effect of modulation of the control voltage as on propagation in the optical fiber constriction. In all cases, activation of modulation increased power, and the recorded spectral characteristic carried the set modulation of steering voltage. To fully illustrate the changes, the spectral characteristics are plotted in a chart in Figure 6. The modulation of 2 Hz for complete reorientation was set to 160 V.

Doping with magnetic NPs significantly increased the power difference between modulated and non-modulated signals (Figure 6). The most significant change was visible for 0.1 wt % and the lowest differences were observed to pure LC 6CHBT. The effect of the magnetic field on pure LC of 6CHBT was negligible, and the differences with and without the magnetic field were the same. Doping the LC with Fe_3O_4 NPs changed the properties, causing a reduction in the total power propagated through the sensor but increasing the dynamic response inflicted on the cell by the electric field. In Figure 5, we present a comparison of the differences in dynamic change during the modulation of electric signals without and with an external magnetic field. The calculated dynamic change for pure 6CHBT for both cases without and with a magnetic field was similar and equal to 2.63 dBm. By contrast, for 6CHBT + 0.1 wt % Fe_3O_4 NPs, these values were equal to 5.66 dBm and 5.58 dBm, respectively, while for 6CHBT + 0.5 wt% Fe_3O_4

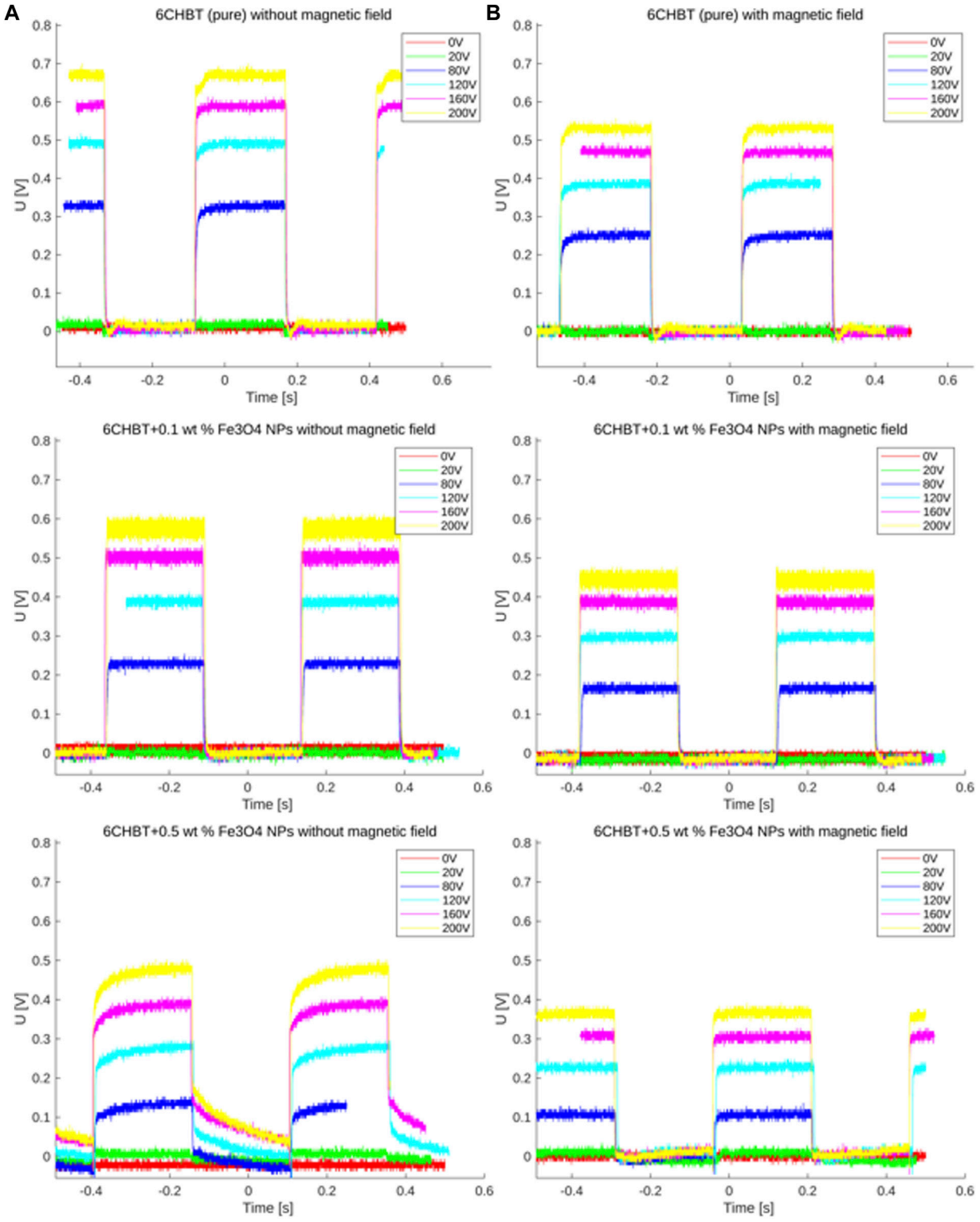

FIGURE 7
Time courses obtained for a steering voltage range of 0–200 V at room temperature (25°C) without **(A)** and with **(B)** the external magnetic field applied. The top row shows results obtained for 6CHBT (pure), the middle row shows 6CHBT + 0.1 wt% Fe_3O_4 NPs, and the bottom row shows 6CHBT + 0.5 wt% Fe_3O_4 NPs.

NPs, they were equal to 3.27 dBm and 3.54 dBm, respectively. The calculations for all graphs were based on data with uncertainty in the reading equal to 0.02 dBm. The doping with 0.1 wt% Fe_3O_4 NPs increased the dynamic response two times, whereas for 0.5 wt% Fe_3O_4 NPs, the dynamic response increased about 1.5 times.

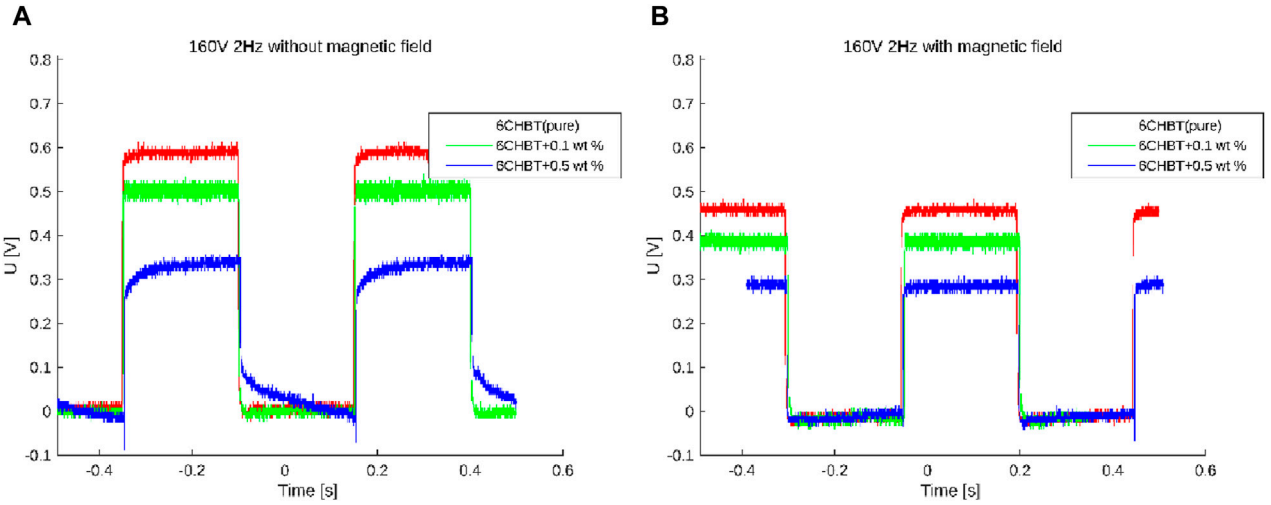

FIGURE 8
Time courses obtained for a steering voltage of 160 V and modulation frequency 2 Hz at room temperature (25°C) for 6CHBT (pure), 6CHBT +0.5 wt% Fe_3O_4 NPs, and 6CHBT + 0.1 wt% Fe_3O_4 NPs under the following conditions: **(A)** without a magnetic field; **(B)** with a magnetic field.

TABLE 2 Switch ON/OFF, overdrive, and relaxation times for 6CHBT (pure), 6CHBT +0.5 wt% Fe_3O_4 NPs, and 6CHBT + 0.1 wt% Fe_3O_4 NPs under the following conditions: without/with a magnetic field. All measurements and calculations are carried out with an accuracy of up to 2 ms.

		6CHBT (pure)	6CHBT + 0.1 wt% Fe_3O_4	6CHBT + 0.5 wt% Fe_3O_4
Switch ON time [ms]*	Without magnetic field	27	14	224
	With magnetic field	23	15	24
Switch OFF time [ms]	Without magnetic field	39	33	1157
	With magnetic field	29	22	19
Overdrive time *[ms]	Without magnetic field	174	62	677
	With magnetic field	154	**11**	**61**
Relaxation time [ms]	Without magnetic field	203	226	1010
	With magnetic field	180	**95**	**109**

Next, we carried out measurements of the time answer for modulation provided due to the proposed arrangements described in the section 2.3 Technology (Figure 4). The bottom picture in Figure 7 presents the time courses obtained for a steering voltage range of 0–200 V at room temperature for the described free mixtures of pure 6CHBT, 6CHBT + 0.1 wt% Fe_3O_4 NPs, and 6CHBT + 0.5 wt% Fe_3O_4 NPs without and with the magnetic field.

A significant increase in the propagating light beam was evident for all cases as the voltage increased. The addition of NPs resulted in a power reduction. The largest change was recorded between pure 6CHBT and 0.1 wt% Fe_3O_4 NPs. The change was much smaller for added 0.1 wt% compared to 0.5 wt% Fe_3O_4 NPs. This loss is due to the interaction of the leaking light beam with the NPs dispersed in the LC and to the formation of inhomogeneities in the molecule alignment in the volume of the LC. Placing the samples in a magnetic field caused an additional power decrease for all measurements. The decrease in power might have to do with the alignment of the NPS according to the field lines and the formation of a distorted LC layer around them with a different average RI, which directly affected propagation. Figure 8 compares time courses obtained for a steering voltage of 160 V and modulation of 2 Hz without and with magnetic field at room temperature.

Based on the obtained results, Table 2 presents the measured times of switch ON and switch OFF, and the times of complete reorientation of molecules (overdrive) and relaxation times of molecules of the investigated devices. As a switch ON (OFF) time, we assumed the time required for a change in the light transmission through the investigated LC cell from 10% to 90% (or *vice versa*) of its maximal value when the steering voltage was switched ON (or OFF). Additionally, we calculated the delay times of ON and OFF in which the measured signal achieved a stable constant maximum or minimum power value after modulation change. These parameters were connected with total overdrive and/or relaxation of LC molecules in the whole volume of measurement cell to the final or initial position.

The admixture of magnetic NPs caused a decrease in power, which was related to the arrangement of the NPs around the taper, causing absorption or dispersion of the leaking light. The admixture

of 0.1 wt% of NPs enhanced the time of complete reorientation when compared to the pure LC setup without a magnetic field. For 0.5 wt% of NPs in a setup without a magnetic field, the times of complete reorientation of molecules between ON and OFF times were significantly worse than it was for pure LC. By applying a magnetic field for both cells with different admixture levels of NPs caused the ON and OFF times to be shorter than it was for pure LC. In all cases, we saw a power reduction but at the same time, a reduction in overdrive and relaxation times.

As can be seen from Table 2, an addition of 0.1 wt% of Fe_3O_4 NPs caused a decrease in switch ON and switch OFF time for both cases without and with magnetic field compared to pure LC. The decrease in times is in the order of 20%–30%. For the case of the addition of 0.5 wt% of Fe_3O_4 NPs without a magnetic field, the times of switch ON and switch OFF were several orders of magnitude larger than were for pure LC. This could be the effect of the arbitrary arrangement of nanoparticles and their high concentration. As a result, the molecules of LCs do not align in accordance with the field lines throughout the volume, which affects the average distribution of the RI and at the same time increases the loss in the propagation of the beam. In this case, the magnetic field caused a significant reduction in time for this case. Times were similar (ON time) or lower (OFF time) than they were in a pure 6CHBT. Considering the liquid crystalline mixture of 0.5 wt% of Fe_3O_4 NPs alone, the application of a magnetic field results in a several-fold reduction in ON and OFF times. In this case, the proposed solution can be tentatively considered a magnetic field sensor. Such a significant change might result from the formation of layers in an LC with different RIs (different orientations of LC molecules) around the nanoparticles aligned along the magnetic field force lines, and it additionally results in the maintenance of the proper orientation of the molecules. The highest decreasing times were observed for 0.5 wt% of Fe_3O_4 NPs in all calculated ON and OFF times and the complete reorientation and release of molecules in the LC when the magnetic field was used. A significant decrease of power in a whole range could be observed for such concentrations, which was strictly connected to the absorption and dispersion of light beams on NPs.

Furthermore, when considering the changes in overdrive and relaxation times, it should be noted that the times with a magnetic field are more than 50% less than they are for pure LC 6CHBT for each degree of admixture of NPs. The admixture of 0.1 wt% of Fe_3O_4 NPs results in a shortening of the full overdrive time by more than 10 times than that for pure LC. For the system without a magnetic field, the results obtained for the doping of 0.1 wt% of Fe_3O_4 NPs show that the overdrive time is half as long and the relaxation time is at a similar level. For doping with 0.5 wt% of Fe_3O_4 NPs, both times are about five times longer than they are for pure LC 6CHBT. For the presented results, it can be noticed that the sensitivity of this device is strictly connected with the parameters of the used LC and built measurement systems. The visible influence of the steering voltage for a 40-μm cell can be observed for 20 V; for this voltage, the orientation of the LC molecules starts to affect light in the taper. For the range of steering voltages and the applied magnetic field, sensitivity is strictly connected with the accuracy of parameters of the optical spectrum analyzer and can be calculated as 0.02 dBm per 1 V. About the time measurement for a single wavelength, the sensitivity of this measurement was calculated for 2 ms for each change of applied field, electric or magnetic one. Additionally for the magnetic field, there was only the measurement of influence of ON/OFF of the magnetic field and the sensitivity connected with the resolution of the applied measurement.

When considering the most important limitations on the use of LCs and the proposed solution, it is important to, first of all, note the limitations related to the properties of the 6CHBT LC and their response speed to a given signal, which is limited to single tens of hertz, additional difficulties may be agglomerations of nanoparticles, which may occur over time. In future research, we will focus on the study and limits of magnetic field detection on a given system, and temperature limit constraints.

4 Conclusion

We present a continuation of our previous works, showing the possibilities of manufacturing optical devices using two technologies: TOF and LCs with different NPs. As can be seen, the use of different types of nanoparticles changes the parameters of LC introduction, and depending on the nanoparticles used, there are changes in both the propagation and ability to control the LCs by electric voltage (better electrical conductivity), temperature (increased heat capacity and formation of crystallization centers), or as described in this article, a magnetic field (changes in the position of nanoparticles in accordance with the lines of force of the magnetic field, causing a change in the RI of the LC). It should also be noted that the results presented here are for magnetic nanoparticles that are sensitive to magnetic fields and allow additional overdriving and changing of LC parameters. Referring to the presented results, it should be noted that most of the bulk magnetite is ferrimagnetic. That means it preserves magnetic properties after the removal of the external magnetic field (hysteresis). However, magnetite nanoparticles of core size below 20 nm perform no hysteresis within the external magnetic field. According to XRD and SEM analysis, the NPs used in the research are most likely single-crystal particles (nanocrystals) of size approximately 7 nm. Such particles are superparamagnetic, and each particle behaves as a single magnetic domain. Therefore, nanoparticles in our system can react immediately to the presence and removal of the external magnetic field, this being the reason for using Fe_3O_4 nanoparticles. This article focuses on the possibility of controlling the switching times and correction of overdrive and relaxation times by a magnetic field in an LC cell doped with magnetic Fe_3O_4 NPs at room temperature. The addition of sufficient magnetic NPs reduces the switching time of the created cell, and the effect can be multiplied by applying a magnetic field. The increase of doped NPs causes an increase in interaction with the magnetic field over ten times, simultaneously increasing losses in the whole range of investigated light. Appropriate doping improves the working parameters for signal detection with different switching ON/OFF times. It should be mentioned that the optimum admixture value for optical measurement is close to the 0.1 wt% of NPs, which modifies LC material parameters and influences light propagating in the whole structure in a wide range. The connection of LCs with NPs allows for significant changes in their optical parameters, such as the effective RI (medium molecule's director) and overdrive and relaxation times, which depend on the possibilities of work for

a higher frequency. In addition, with the help of magnetic NPs, light propagation can be influenced by indirect factors such as the magnetic field. The application of the field influences the alignment of the NPs with the field lines, changing the molecules' position around the taper and, thus, the average RI, which directly influences light propagation. The results show the possibilities of producing compact, miniaturized systems for commercial application, which can be tuned by applying various external stimuli.

Data availability statement

The raw data supporting the conclusion of this article will be made available by the authors, without undue reservation.

Author contributions

MN: writing—original draft, visualization, validation, investigation, and data curation. KS: writing—original draft, visualization, supervision, resources, methodology, investigation, formal analysis, data curation, and conceptualization. NP: writing—original draft, visualization, resources, investigation, and formal analysis. AP: writing—review and editing, resources, and formal Analysis. JP: writing—review and editing, resources, and funding acquisition. RZ: writing—review and editing, visualization, and resources. JD: writing—review and editing and resources. PK: writing—review and editing, supervision, and resources. LJ: writing—review and editing, resources, and funding acquisition.

Funding

The authors declare that financial support was received for the research, authorship, and/or publication of this article. This work was supported by the Program of the Republic of Poland—Research Grant MUT project no UGB 22-725. Works done by JP and RZ were supported by the National Science Center, Poland, within grant OPUS 2019/35/B/ST5/03229.

Conflict of interest

The authors declare that the research was conducted in the absence of any commercial or financial relationships that could be construed as a potential conflict of interest.

Acknowledgments

The authors thank Michał Folga for the help with the synthesis and characterization of the nanoparticles.

Publisher's note

References

Ahamed, M. S., AlSalhi, M. S., and Siddiqui, M. (2010). Silver nanoparticle applications and human health. *Clin. Chim. Acta* 411, 1841–1848. doi:10.1016/j.cca.2010.08.016

Al-Qazwini, Y., Noor, A. S. M., Yaacob, M. H., Harun, S. W., and Mahdi, M. A. (2015). Experimental realization and performance evaluation of refractive index SPR sensor based on unmasked short tapered multimode-fiber operating in aqueous environments. *Sensors Actuators A Phys.* 236, 38–43. doi:10.1016/j.sna.2015.10.030

Baldini, F., Giannetti, A., Mencaglia, A. A., and Trono, C. (2008). Fiber optic sensors for biomedical applications. *Curr. Anal. Chem.* 4, 378–390. doi:10.2174/157341108785914880

Blanc, W., Lu, Z., Robine, T., Pigeonneau, F., Molardi, C., and Tosi, D. (2022). Nanoparticles in optical fiber, issue and opportunity of light scattering [Invited]. *Opt. Mat. Express* 12, 2635–2652. doi:10.1364/OME.462822

Brambilla, G. (2010). Optical fibre nanowires and microwires: review. *J. Opt.* 12, 1–19. doi:10.1088/2040-8978/12/4/043001

Budaszewski, D., Chychłowski, M., Budaszewska, A., Bartosewicz, B., Jankiewicz, B., and Woliński, T. R. (2019). Enhanced efficiency of electric field tunability in photonic liquid crystal fibers doped with gold nanoparticles. *Opt. Express* 27, 14260. doi:10.1364/oe.27.014260

Butt, M. A., Voronkov, G. S., Grakhova, E. P., Kutluyarov, R. V., Kazanskiy, N. L., and Khonina, S. N. (2022). Environmental monitoring: a comprehensive review on optical waveguide and fiber-based sensors. *Biosensors* 12, 1038. doi:10.3390/bios12111038

Chen, L., Leng, Y.-K., Liu, B., Liu, J., Wan, S.-P., Wu, T., et al. (2020). Ultrahigh-sensitivity label-free optical fiber biosensor based on a tapered singlemode- No core-singlemode coupler for Staphylococcus aureus detection. *Sensors Actuators B Chem.* 320, 128283. doi:10.1016/j.snb.2020.128283

Chen, Y., Sun, W., Zhang, Y., Liu, G., Luo, Y., Dong, J., et al. (2019). Magnetic nanoparticles functionalized few-mode-fiber-based plasmonic vector magnetometer. *Nanomater. (Basel)* 9 (5), 785. PMID: 31121934; PMCID: PMC6567098. doi:10.3390/nano9050785

Das, P., Behera, B. C., Dash, S. P., Ajith, N. E. S. R., Kiruthiga Devi, B., Sahoo, N. K., et al. (2022). Co_3O_4 magnetic nanoparticles-coated optical fibers for sensing sialic acid tripathy. *ACS Appl. Nano Mater.* 5 (7), 8973–8981. doi:10.1021/acsanm.2c01172

Dudek, M., Kujawińska, M., Parat, V., Baethge, G., Michalska, A., Dahmani, B., et al. (2014). Tomographic and numerical studies of polymer bridges between two optical fibers for telecommunication applications. *Opt. Eng.* 53 (1), 016113. doi:10.1117/1.oe.53.1.016113

Dufour, A., Bsawmaii, L., Jamon, D., Marin, E., Neveu, S., Reynaud, S., et al. (2020). "Micro-structured optical fiber functionalization with magnetic nanoparticles doped sol-gel matrix: application to an all-fiber magnetic field sensor," in *Optical fiber sensors conference 2020 special edition*. Editors G. Cranch, A. Wang, M. Digonnet, and P. Dragic (Washington: Optica Publishing Group).

Frazão, O., Santos, J. L., Ara'ujo, F. M., and Ferreira, L. A. (2008). Optical sensing with photonic crystal fibers. *Laser and Photonics Rev.* 2, 449–459. doi:10.1002/lpor.200810034

Fu, X., Li, D., Zhang, Y., Fu, G., Jin, W., and Bi, W. (2022). High sensitivity refractive index sensor based on cascaded core-offset splicing NCF-HCF-NCF structure. *Opt. Fiber Technol.* 68, 102791. doi:10.1016/j.yofte.2021.102791

Guo, Q., Zhu, Y., Shan, T., Pan, X., Liu, S., Xue, Z., et al. (2021). Intensity-modulated directional torsion sensor based on a helical fiber taper. *Opt. Mater. Express* 11, 80–88. doi:10.1364/ome.411139

Hsu, C. J., Lin, L. J., Huang, M. K., and Huang, C. Y. (2017). Electro-optical effect of gold nanoparticle dispersed in nematic liquid crystals. *Crystals* 7, 287–310. doi:10.3390/cryst7100287

Huang, L., Lin, S., Xu, Z., Zhou, H., Duan, J., Hu, B., et al. (2020). Fiber-based energy conversion devices for human-body energy harvesting. *Adv. Mater.* 32, 1902034. doi:10.1002/adma.201902034

Jadżyn, J., Hellemans, L., Czechowski, G., and Legrand, Ch. (2010). Douai Dielectric and viscous properties of 6CHBT in the isotropic and nematic phases. *Liq. Cryst.* 1, 613–619. doi:10.1080/026782900202453

Katsunari, O. (2006). *Wave theory of optical waveguides. Fundamentals of optical waveguides*. Londyn: Academic Press, 1–12.

Kim, H.-M., Park, J.-H., and Lee, S.-K. (2019). Fiber optic sensor based on ZnO nanowires decorated by Au nanoparticles for improved plasmonic biosensor. *Sci. Rep.* 9, 15605. doi:10.1038/s41598-019-52056-1

Korec, J., Stasiewicz, K. A., Strzeżysz, O., Kula, P., and Jaroszewicz, L. R. (2019). Electro-steering tapered fiber-optic device with liquid crystal cladding. *J. Sensors* 2019, 1–11. doi:10.1155/2019/1617685

Korposh, S., James, S., Lee, S., and Tatam, R. (2019). Tapered optical fibre sensors: current trends and future perspectives. *Sensors* 19, 2294. doi:10.3390/s19102294

Kurzych, A. T., Jaroszewicz, L. R., and Kowalski, J. K. (2022). Development of three-Axis fibre-optic seismograph for direct and autonomous monitoring of rotational events with perspective of historical review. *Sensors* 22 (22), 8902. doi:10.3390/s22228902

Kurzych, A. T., Jaroszewicz, L. R., Kowalski, J. K., and Sakowicz, B. (2020). Investigation of rotational motion in a reinforced concrete frame construction by a fiber optic gyroscope. *Opto-Electronics Rev.* 28 (2), 69–73. doi:10.24425/opelre.2020.132503

Lacková, V., Schroer, M. A., Hähsler, M., Zakutanská, K., Behrens, S., Kopčanský, P., et al. (2024). The collective ordering of magnetic nanoparticles in a nematic liquid crystal. *J. Magnetism Magnetic Mater.* 589, 171616. doi:10.1016/j.jmmm.2023.171616

Larsen, T. T., Bjarklev, A., Hermann, D., and Broeng, J. (2003). Optical devices based on liquid crystal photonic bandgap fibres. *Opt. Express* 11, 2589–2596. doi:10.1364/oe.11.002589

Layeghi, A., and Latifi, H. (2018). Tunable ferrofluid magnetic fiber sensor based on nonadibatic tapered hi-Bi fiber in fiber loop mirror. *J. Light. Technol.* 36, 1097–1104. doi:10.1109/JLT.2017.2781623

Li, J. (2020). A review: development of novel fiber-optic platforms for bulk and surface refractive index sensing applications. *Sensors Actuators Rep.* 2 (1), 100018. doi:10.1016/j.snr.2020.100018

Li-hui, F., and Junfeng, D. (2023). Mixed oil detection method based on tapered fiber SPR sensor. *Opt. Fiber Technol.* 78, 103322. doi:10.1016/j.yofte.2023.103322

Lohse, S. E., and Murphy, C. J. (2012). Applications of colloidal inorganic nanoparticles: from medicine to energy. *J. Am. Chem. Soc.* 134, 15607–15620. doi:10.1021/ja307589n

Luo, L., Pu, S., Tang, J., Zeng, X., and Lahoubi, M. (2015). Highly sensitive magnetic field sensor based on microfiber coupler with magnetic fluid. *Appl. Phys. Lett.* 106, 193507. doi:10.1063/1.4921267

Markos, Ch., Travers, J. C., Abdolvand, A., Eggleton, B. J., and Bang, O. (2017). Hybrid photonic-crystal fiber. *Rev. Mod. Phys.* 89, 045003. doi:10.1103/revmodphys.89.045003

Miao, Y., Liu, Bo, Zhang, K., Liu, Y., and Zhang, H. (2011). Temperature tunability of photonic crystal fiber filled with Fe_3O_4 nanoparticle fluid. *Appl. Phys. Lett.* 98 (2), 021103. doi:10.1063/1.3540647

Moś, J. E., Stasiewicz, K. A., and Jaroszewicz, L. R. (2022). Investigation of transmission properties of a tapered optical fibre with gold nanoparticles liquid crystal composite cladding. *Opto-Electronics Rev.* 30, 4. doi:10.24425/opelre.2022.143936

Nealon, G. L., Greget, R., Dominguez, C., Nagy, Z. T., Guillon, D., Gallani, J. L., et al. (2012). Liquid-crystalline nanoparticles: hybrid designand mesophase structures. *Beilstein J. Org. Chem.* 8, 349–370. doi:10.3762/bjoc.8.39

Orlandi, S., Benini, E., Miglioli, I., Evans, D. R., Reshetnyak, V., and Zannoni, C. (2016). Doping liquid crystals with nanoparticles. A computer simulation of the effects of nanoparticle shape. *Phys. Chem. Chem. Phys.* 18, 2428–2441. doi:10.1039/c5cp05754j

Petcharoen, K., and Sirivat, A. (2012). Synthesis and characterization of magnetite nanoparticles via the chemical Co-precipitation method. *Mater. Sci. Eng. B* 177 (5), 421–427. doi:10.1016/j.mseb.2012.01.003

Scherrer, P. (1918). "Bestimmung Der Inneren Struktur Und Der Größe von Kolloidteilchen Mittels Röntgenstrahlen," in *Kolloidchemie ein lehrbuch* (Berlin, Heidelberg: Springer), 387–409. doi:10.1007/978-3-662-33915-2_7

Sengupta, A. (2013). *Liquid crystal theory. Topological microfluidics: nematic liquid crystals and nematic colloids in microfluidic enviroment*. Switzeland: Springer, 7–34.

Shi, F., Bai, X., Wang, F., Pang, F., Pu, S., and Zeng, X. (2017). All-fiber magnetic field sensor based on hollow optical fiber and magnetic fluid. *IEEE Sensors J.* 17, 619–622. doi:10.1109/JSEN.2016.2636879

Shi, F., Luo, Y., Che, J., Ren, Z. J., and Peng, B. J. (2018). Optical fiber F–P magnetic field sensor based on magnetostrictive effect of magnetic fluid. *Opt. Fiber Technol.* 43, 35–40. doi:10.1016/J.YOFTE.2018.01.008

Škarabot, M., Ryzhkova, A. V., and Muševič, I. (2018). Interactions of single nanoparticles in nematic liquid crystal. *J. Mol. Liq.* 267, 384–389. doi:10.1016/j.molliq.2018.01.068

Stasiewicz, K. A., Jakubowska, I., and Dudek, M. (2022a). Detection of organosulfur and organophosphorus compounds using a hexafluorobutyl acrylate-coated tapered optical fibers. *Polymers* 14, 612. doi:10.3390/polym14030612

Stasiewicz, K. A., Jakubowska, I., Moś, J. E., Marć, P., Paczesny, J., Zbonikowski, R., et al. (2022b). Optical properties of a tapered optical fiber coated with alkanes doped with Fe_3O_4 nanoparticles. *Sensors* 22, 7801. doi:10.3390/s22207801

Taha, B. A., Ali, N., Sapiee, N. M., Fadhel, M. M., Mat Yeh, R. M., Bachok, N. N., et al. (2021). Comprehensive review tapered optical fiber configurations for sensing application: trend and challenges. *Biosensors* 11, 253. doi:10.3390/bios11080253

Tian, Y., Wang, W., Wu, N., Zou, X., and Wang, X. (2011). Tapered optical fiber sensor for label-free detection of biomolecules. *Sensors* 11, 3780–3790. doi:10.3390/s110403780

Tiwari, D., Mullaney, K., Korposh, S., James, S. W., Lee, S.-W., and Tatam, R. P. (2017). An ammonia sensor based on Lossy Mode Resonances on a tapered optical fibre coated with porphyrin-incorporated titanium dioxide. *Sensors Actuators B Chem.* 242, 645–652. doi:10.1016/j.snb.2016.11.092

Urbanski, M. (2015). On the impact of nanoparticle doping on the electro-optic response of nematic hosts. *Liq. Cryst. Today* 24, 102–115. doi:10.1080/1358314x.2015.1059586

Veilleux, C., Black, R. J., Lapierre, J., and Reeves, L. W. (1990). Nematic liquid crystal clad tapered optical fiber with temperature sensing properties. *J. Appl. Phys.* 67, 6648–6653. doi:10.1063/1.345098

Wang, S., Feng, S., Wu, S., Wang, Q., and Zhang, L. (2018). Hight sensitive temperature sensor based on gain competition mechanism using graphene coated microfiber. *IEEE Photonics J.* 10, 6802008. doi:10.1109/JPHOT.2018.2827073

Woliński, T. R., Siarkowska, A., Budaszewski, D., Chychłowski, M., Czapla, A., Ertman, S., et al. (2017). Recent advances in liquid-crystal fiber-optics and photonics. *Emerg. Liq. Cryst. Technol. XII* 10125, 101250W. doi:10.1117/12.2261115

Zhang, S., Peng, Y., Wei, X., and Zhao, Y. (2022). High-sensitivity biconical optical fiber SPR salinity sensor with a compact size by fiber grinding technique. *Measurement* 204, 112156. doi:10.1016/j.measurement.2022.112156

Zhao, Y., Zhao, H., Lv, R., and Zhao, J. (2019). Review of optical fiber mach–zehnder interferometers with micro-cavity fabricated by femtosecond laser and sensing applications. *Opt. Lasers Eng.* 117, 7–20. doi:10.1016/j.optlaseng.2018.12.013

Zheng, Y., Dong, X., Chan, C. C., Shum, P. P., and Su, H. (2015). Optical fiber magnetic field sensor based on magnetic fluid and microfiber mode interferometer. *Opt. Commun.* 336, 5–8. ISSN 0030-4018. doi:10.1016/j.optcom.2014.09.026